

See discussions, stats, and author profiles for this publication at: <https://www.researchgate.net/publication/388129896>

# Design of a Piecewise–Stiffening Nonlinear Energy Sink for Torsional Vibration Attenuation

Preprint · January 2025

DOI: 10.2139/ssrn.5101506

---

CITATIONS

0

---

READS

20

3 authors, including:



[Harikrishnan Venugopal](#)  
Ghent University

6 PUBLICATIONS 6 CITATIONS

[SEE PROFILE](#)



[Kevin Dekemele](#)  
Ghent University

52 PUBLICATIONS 549 CITATIONS

[SEE PROFILE](#)

# Design of a Piecewise-Stiffening Nonlinear Energy Sink for Torsional Vibration Attenuation

Harikrishnan Venugopal<sup>a,\*</sup>, Mia Loccufer<sup>a</sup>, Kevin Dekemele<sup>a</sup>

<sup>a</sup>*Ghent University, Department of Electromechanical, Systems and Metal Engineering, Tech Lane Ghent Science Park- Campus A-46, Ghent, 9052, Belgium*

---

## Abstract

Torsional vibrations are of vital importance in rotating machinery, with demands of better performance and material savings potentially inducing resonance conditions. A robust and effective vibration attenuation solution is offered by the Nonlinear Energy Sink (NES). In this research, a 2-DOF torsional host structure is attached to an NES having piecewise-linear stiffness. The design of the NES is optimized for minimal stresses in the local members while avoiding local resonances. The coupled NES-host system is analyzed using Complexification-Averaging of the first-order and validated by experimental and numerical means. While existing research is primarily focused on the resonant response, a study of the possible bifurcations is also needed. In this regard, the experimental validation reveals typical nonlinear behavior of quasi-periodic responses and isolated resonance curves, also with a significant attenuation at resonance. As such, a complete toolchain is developed from analytical tuning, material strength optimization and realization, that can be applied to a wide range of torsional vibration applications.

### Keywords:

Nonlinear Energy Sink (NES), Torsional vibration, Complexification-Averaging, Design optimization, Piecewise nonlinearity

---

## 1. Introduction

Attenuation of torsional vibration is of great importance in the field of turbomachinery and transmission design. Industry trends of the current decade have led to a demand for increased fuel efficiency and performance, thereby creating a demand for lightweight constructions; development of design optimization is a product of this demand. However, this trend places the system's dynamics close to their resonances. This is especially crucial for rotating machinery as torsion-induced shear stress has a lower fatigue limit for failure compared to bending/tensile stress. A selection of research in torsional vibration analysis and material fatigue is presented in [1, 2, 3, 4, 5]. Suitable care needs to be taken during the design stage to mitigate these issues.

---

\*Corresponding author

Email address: harikrishnan.venugopal@ugent.be (Harikrishnan Venugopal)

A potential solution is to add vibration absorbers tuned to absorb the resonant vibrations of the primary/host system. The earliest form of the Tuned Mass Damper (TMD) as passive auxiliary attachment was proposed by Frahm[6] and further developed by Den Hartog[7], where the latter also proposed an optimal damping criterion. Additionally, the field of vibration mitigation saw the rise of electromechanical actuation, thus founding active [8, 9, 10, 11] and semi-active [12, 13, 14, 15, 16] vibration absorbers. Though, a well-designed control strategy promises excellent vibration attenuation, the need for actuation is a disadvantage for such devices. Concerning torsional vibrations, several TMD variations have been explored in the past, namely, the Dual-Mass Flywheel[17], the speed-dependent absorbers[18, 19] and the damped pulley absorber[20]. A major disadvantage of a TMD is its narrow frequency band of attenuation and the presence of side-resonances. While having great commercial success, it was identified that introducing nonlinear elements to the absorber could greatly improve its robustness and range of operation.

The nonlinear vibration absorber, also referred to as Nonlinear Energy Sink (NES), offers several advantages over its linear counterparts: (1) it can work effectively even when the system has undergone slight perturbations to its parameters, and (2) the nonlinearity allows the device to attenuate multiple resonant frequencies of the host system[21, 22, 23, 24]. The former property of ‘de-tuning’ supports its robustness and the latter supports its role as a broadband absorber. The NES cannot completely attenuate the resonant response as done by a TMD, but it avoids the side resonances. The NES has a variable natural frequency dependent on the magnitude of excitation, and thus can self-tune to the frequency of the host system. For transient excitations, the NES initiates Targeted Energy Transfer (TET), an irreversible pumping of energy to the NES, where the energy is then dissipated via damping[25, 26, 24, 27]. For harmonic excitations, at 1:1 resonance a quasi-periodic response similar to relaxation oscillations occur [22, 21]. In general, for the nonlinear system, several potential responses can be obtained at a single exciting frequency depending on the initial conditions. Such bifurcating responses need to be accurately characterised for an effective implementation of the NES. First introduced by Vakakis[28], the NES technology has gained a lot of popularity in the recent times. Examples of implementations of NES are also vast, with notable advancements in the domain of seismic vibration mitigation[29, 30, 31, 32], aerospace technology[33, 34, 35], and mechanical engineering [36, 37, 38]. An in-depth review of the NES technology is given in [39, 40].

A number of nonlinear stiffness and damping variations of the NES have been studied for their potential. In this aspect, the cubic[41, 23, 42], the softening[43, 44, 45], the saturating[43, 46], the periodic[47, 48], the bistable[49, 50, 51, 52, 32, 53], and the tristable[54, 55, 56] stiffness characteristics are of interest. Additionally, a general framework for analysis of non-smooth NES has also been explored by Lamarque et al.[57]. The type of nonlinearity chosen affects the order of attenuation of resonances and its threshold energy for initiating TET. Similarly, nonlinear damping has also seen a variety in its kind[58, 59, 50]. Concerning solution methods, analytical techniques such as Harmonic Balancing (HB)[60] and Complexification-Averaging (CxA)[61, 24, 62] method has achieved great popularity in the analysis of nonlinear systems, as they offer better insights compared to their numerical counterparts. There have been several recent realizations of NESs as a means for torsional vibration attenuation. In this matter, an early research has been presented by Haris et al.[63] wherein a cubic, a 5<sup>th</sup> order and a vibro-impact NES is explored for their

effectiveness in attenuating torsional vibrations. An experimental-cum-numerical validation of the NES efficacy is also presented by the same author[64]. Later, Cao et al. presents a piecewise-linear stiffness NES attached to an inerter mechanism offering significant resonant vibration suppression with low NES mass[65]. Similar concepts of inducing nonlinearity in the NES has been used by the same authors to attenuate both transient and harmonic loads[66, 67], and also to design a multi-stable NES[68]. Furthermore, novel designs of inducing nonlinearity by means of permanent magnets[69, 70] and via particle dampers[71] have also been studied; significant reductions in vibration amplitude and suppression time is reported here. A recent research by Cao et al. also presents a piecewise-linear NES design capable of multi-modal torsional attenuation[72]. The aforementioned research showcase design concepts but do not elaborate on the structural strength aspects or expand on optimal configurations for their durability. Furthermore, analytical techniques are not being used to fully explore the dynamical behaviour and to validate the design's performance.

In this paper, a variation of the design from Cao et al.[67] is chosen, but with a focus on obtaining an analytical solution for the forced response, tuning of the NES stiffness, and on the practical aspects of strength/durability of the design which was missing from previous works. As such, a complete toolchain is presented that, from analytical model to realization, can be easily adapted to other torsional systems. Firstly, a dynamic model of the experimental setup is formulated, and an analytical solution is obtained using the CxA method. Further, the design of the NES and formulation of its design optimization problem is discussed. An experimental validation is conducted, where it is found that the experimental results match well with the analytical predictions. It is also important, apart from showcasing the advantages of a tuned NES, to explore bifurcating responses which can be detrimental to its overall performance.

## 2. Dynamic model description

The vibration response of a structure with a NES is described through the study of its dynamic model. The primary system where the toolchain will be applied is a benchmark 2-DOF torsional vibration setup mounted vertically, and the NES is attached to the  $I_2$  inertia, as shown in Fig 1. The methodology described however is applicable to  $n$ -DOF systems as well.

### 2.1. Equations of motion

The vibration of a torsional  $n$ -DOF primary system with NES is described by the following Equations Of Motion (EOM):

$$\begin{aligned} \mathbf{I}\ddot{\theta} + \mathbf{C}\dot{\theta} + \mathbf{K}\theta + \delta_\ell(I_{\text{na}}\ddot{\theta}_{\text{na}}) &= \mathbf{F} \cos(\omega t) \\ I_{\text{na}}\ddot{\theta}_{\text{na}} + c_{\text{na}}(\theta_{\text{na}} - \theta_\ell) + k_{\text{na}}(\theta_{\text{na}} - \theta_\ell)^3 &= 0 \end{aligned} \quad (1)$$

Where  $\theta \in \mathbb{R}^{n \times 1}$  is the angular displacement vector,  $\mathbf{I} \in \mathbb{R}^{n \times n}$  is the rotational inertia matrix,  $\mathbf{C} \in \mathbb{R}^{n \times n}$  the damping matrix,  $\mathbf{K} \in \mathbb{R}^{n \times n}$  the stiffness matrix,  $\delta_\ell \in \mathbb{R}^{n \times 1}$  the NES connection vector, which is 1 at the connection DOF of the NES and 0 elsewhere and  $\mathbf{F}$  the force vector. The absorber parameters are the absorber angular displacement  $\theta_{\text{na}}$ , the

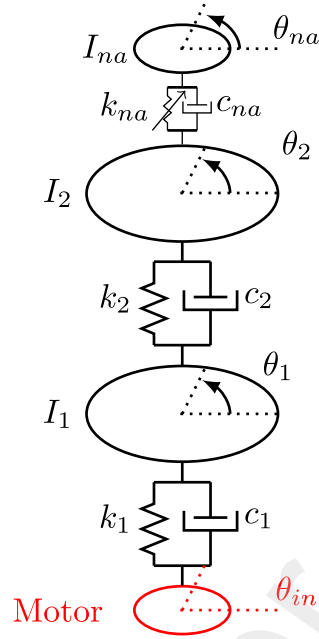


Figure 1: Simplified model of the coupled NES-host system. The inertias  $I_1$  and  $I_2$  form the host, and  $I_{na}$  is the NES inertia. The forcing input is provided by motor as  $\theta_{in}$ .

absorber damping  $c_{na}$  and the absorber nonlinear stiffness  $k_{na}$ . The following eigenvalue problem is obtained from the undamped, unforced linear system:

$$(\mathbf{K} - \mathbf{I}\omega_i^2)\mathbf{e}_i = 0 \quad (2)$$

where  $\omega_i^2$  is the  $i^{th}$  eigenvalue and  $\mathbf{e}_i \in \mathbb{R}^{n \times 1}$  is the  $i^{th}$  eigenvector. In the modal coordinates  $\theta = \mathbf{E}q$ , with  $\mathbf{E} = [\mathbf{e}_1, \mathbf{e}_2, \dots, \mathbf{e}_n]$ , the EOM are:

$$\begin{aligned} I_{q,i}\ddot{q}_i + c_{q,i}\dot{q}_i + k_{q,i}q_i + e_i(\ell)(I_{na}\ddot{\theta}_{na}) \\ = \mathbf{e}_i^T \mathbf{F} \cos(\omega t) \text{ for } i = [1, \dots, n] \quad P \\ I_{na}\ddot{\theta}_{na} + c_{na}(\dot{\theta}_{na} - \dot{\theta}_\ell) + k_{na}(\theta_{na} - \theta_\ell)^3 = 0 \end{aligned} \quad (3)$$

The dynamics is considered around a dominant single mode  $i$ . Rewriting Eq. (3) with the coordinate where the NES is attached to being modified as  $\theta_\ell = q_i e_i(\ell)$ , is then:

$$\begin{aligned} \frac{I_{q,i}}{e_i(\ell)^2} \ddot{\theta}_\ell + \frac{c_{q,i}}{e_i(\ell)^2} \dot{\theta}_\ell + \frac{k_{q,i}}{e_i(\ell)^2} \theta_\ell + (I_{na}\ddot{\theta}_{na}) = \frac{F_m}{e_i(\ell)} \cos(\omega t) \\ I_{na}\ddot{\theta}_{na} + c_{na}(\dot{\theta}_{na} - \dot{\theta}_\ell) + k_{na}(\theta_{na} - \theta_\ell)^3 = 0 \end{aligned} \quad (4)$$

Where  $F_m = \mathbf{e}_i^T \mathbf{F}$  is the modal force. Defining  $\theta_\ell = y$ , the relative absorber motion  $z = \theta_{na} - y$ , dividing Eq. (4) by  $\frac{I_{q,i}}{e_i(\ell)^2}$ :

$$\begin{aligned} \ddot{y} + \varepsilon \xi \omega_i \dot{y} + \omega_i^2 y + \varepsilon(\ddot{z} + \ddot{y}) = \varepsilon \omega_i^2 P \cos(\omega t) \\ \varepsilon(\ddot{z} + \ddot{y}) + \varepsilon \xi_{na} \omega_i \dot{z} + \varepsilon \omega_i^2 \gamma z^3 = 0 \end{aligned} \quad (5)$$

where,

$$\begin{aligned}\varepsilon &= \frac{I_{na}e_i^2(\ell)}{I_{q,i}} & \omega_i^2 &= \frac{k_{q,i}}{I_{q,i}} & \xi &= \frac{c_{q,i}}{I_{na}\omega_i} \\ \xi_{na} &= \frac{c_{na}}{I_{na}\omega_i} & \gamma &= \frac{k_{na}}{I_{na}\omega_i^2} & P &= \frac{F_m}{I_{na}\omega_i^2 e_i(\ell)}\end{aligned}\quad (6)$$

Finally, the time and motion are made dimensionless by the following substitution:

$$\tau = \omega_i t \quad \bar{y} = \sqrt{\gamma} y \quad \bar{z} = \sqrt{\gamma} z$$

Following which Eq. (5) becomes,

$$\begin{aligned}\bar{y}'' + \varepsilon \xi \bar{y}' + \bar{y} + \varepsilon (\bar{z}'' + \bar{y}'') &= \varepsilon \bar{P} \cos(\Omega \tau) \\ \varepsilon (\bar{z}'' + \bar{y}'') + \varepsilon \xi_{na} \bar{z}' + \varepsilon \bar{z}^3 &= 0\end{aligned}\quad (7)$$

where

$$(\cdot)' = \frac{\partial(\cdot)}{\partial \tau} \quad \Omega = \frac{\omega}{\omega_i} \quad \bar{P} = \sqrt{\gamma} P \quad (8)$$

## 2.2. Complexification-Averaging

Complexification-Averaging is performed to study the dynamics on the envelope of vibration, i.e. the slow flow dynamics. The vibrations are assumed to have a single frequency  $\Omega$ . The following complex Manevitch variables [61]  $A$  and  $B$  facilitate this:

$$2A(\tau) \exp(j\tau) = \bar{y} - j \frac{\bar{y}'}{\Omega} \quad 2B(\tau) \exp(j\tau) = \bar{z} - j \frac{\bar{z}'}{\Omega} \quad (9)$$

where  $A$  and  $B$  hold the amplitude and phase modulation. The original variables are then substituted by:

$$\begin{aligned}\bar{y} &= A(\tau) \exp(j\Omega\tau) + A^*(\tau) \exp(-j\Omega\tau) \\ \bar{y}' &= j\Omega (A(\tau) \exp(j\Omega\tau) - A^*(\tau) \exp(-j\Omega\tau)) \\ \bar{y}'' + \Omega \bar{y} &= j2\Omega A' \exp(j\Omega\tau) \\ \bar{z} &= B(\tau) \exp(j\Omega\tau) + B^*(\tau) \exp(-j\Omega\tau) \\ \bar{z}' &= j\Omega (B(\tau) \exp(j\Omega\tau) - B^*(\tau) \exp(-j\Omega\tau)) \\ \bar{z}'' + \Omega \bar{z} &= j2\Omega B' \exp(j\Omega\tau)\end{aligned}\quad (10)$$

Where  $j$  is the imaginary variable and (\*) indicate the complex conjugate. Substituting Eq. (10) into Eq. (7) and keeping only the terms with frequency  $\Omega$  yields:

$$\begin{aligned}j\Omega A' + j\varepsilon \xi \Omega A + (1 - \Omega^2)A + \varepsilon (j\Omega B' - \Omega^2 B + j2\Omega A' - \Omega^2 A) &= \frac{\varepsilon \bar{P}}{2} \\ j2\Omega B' + 2j\Omega A' - \Omega^2 B - \Omega^2 A + \xi_{na} j\Omega B + 3B|B|^2 &= 0\end{aligned}\quad (11)$$

which is basically an averaging procedure over the forcing frequency  $\Omega$ . In steady state ( $A' = B' = 0$ ), Eq. (11) is reduced to:

$$\begin{aligned}j\xi \sqrt{X}A + \sigma A - XB - XA &= \frac{\bar{P}}{2} \\ -XB - XA + \xi_{na} j\sqrt{X}B + 3B|B|^2 &= 0\end{aligned}\quad (12)$$

with  $X = \Omega^2$  and  $\varepsilon\sigma = 1 - X$ . The stability of the steady state solutions is computed using the Jacobian in Appendix A and B. Next, the equations can be manipulated to obtain two equations in  $Z_a = a^2$  and  $Z_b = b^2$  with  $A = \frac{a}{2}e^{j\alpha}$  and  $A = \frac{b}{2}e^{j\beta}$ . The first one is a SIM between  $Z_a$  and  $Z_b$ :

$$X^2 Z_a = Z_b \left( X \xi_{na}^2 + \left( X - \frac{3}{4} Z_b \right)^2 \right) \quad (13)$$

and the second a SIM that relates  $Z_b$  with  $\bar{P}$ :

$$\left[ (X - \sigma) \left( \frac{3}{4} Z_b - X \right) + X \xi_{na} \xi + X^2 \right]^2 Z_b + X \left[ \xi \left( \frac{3}{4} Z_b - X \right) + (\sigma - X) \xi_{na} \right]^2 Z_b = (X \bar{P})^2 \quad (14)$$

Per excitation level  $\bar{P}$ , a frequency response can be computed by first solving Eq. (14) for  $Z_b$  and computing the corresponding  $Z_a$  from Eq. (13), over a range of  $X$ . The maxima and minima of the SIM are important in tuning the absorber stiffness. These are obtained by deriving Eq. (13) w.r.t  $Z_b$  and finding the roots:

$$Z_b^+ = \frac{8}{9} X + \frac{4}{9} \sqrt{X^2 - 3\xi_{na}} \quad (15a)$$

$$Z_b^- = \frac{8}{9} X - \frac{4}{9} \sqrt{X^2 - 3\xi_{na}} \quad (15b)$$

$$Z_a^+ = Z_b^- \left( X \xi_{na}^2 + \left( X - \frac{3}{4} Z_b^- \right)^2 \right) / X^2 \quad (15c)$$

$$Z_a^- = Z_b^+ \left( X \xi_{na}^2 + \left( X - \frac{3}{4} Z_b^+ \right)^2 \right) / X^2 \quad (15d)$$

The inflection points thus obtained are tuned for the optimal NES performance.

### 2.3. Insights from analytical calculations

In this section, the dynamical behaviour of the system is explained in relation to the SIM equations calculated previously. Tracing the response envelopes for a harmonic excitation (Figs. 3a and 3b), both  $a$  and  $b$  increases along the left branch until the maxima ( $\sqrt{Z_b^-}$ ,  $\sqrt{Z_a^+}$ ) is reached, and the response jumps to the branch on the right, inducing the desired regime of Strongly Modulated Response (SMR) [21, 22, 73], where a faster rate of energy dissipation is achieved. At the end of the SMR regime, the system jumps to the left branch and thereafter repeats this response as a limit-cycle oscillation. The SIM of the frequency response from Eqs. (13) and (14) is shown for various forcing levels ( $\bar{P}$ ) in Fig. 2. Around the resonant frequency we see a saturation in the response level as the forcing increases. Additionally, the response is also considered to be unstable. This is indicative of the limit-cycle response as explained by the SIM in Fig. 3a and by a corresponding time simulation of the full EOM (refer Eq. (5)) in Fig. 3b. This infers that the response saturation in the frequency response is dictated by the maxima of the SIM, defined by Eq. (15c) and is plotted as a thin dashed line in Fig. 2. As such, this serves as a design criterion for response suppression to safe levels. However, if the primary system stays below the maxima, then the absorber will not activate. Thus, the SIM limits should be designed also taking the forcing limits into account. At sub-resonant frequencies we observe the inception of a bifurcating, Isolated Resonance Curve (IRC)[74] (or isola) as the forcing amplitude increases.

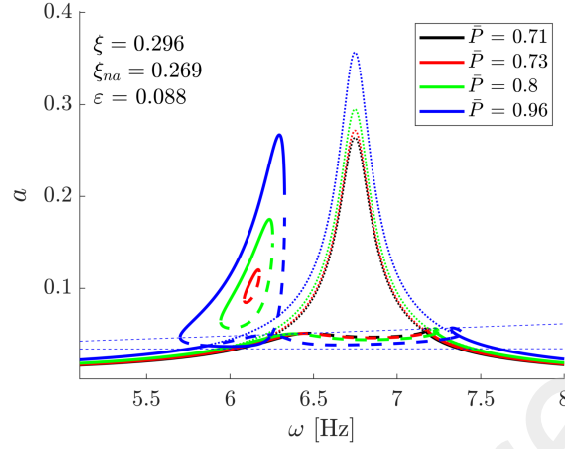


Figure 2: Frequency Response of the NES-host system (stable (—) and unstable (---)) compared to that of the host system (.....); SIM limits are indicated by (- - -). The figure shows the evolution of Isolated Resonance Curves with the increase in forcing. Additionally, the saturation of the 1:1 resonant response is observed.

This detached curve enlarges at higher forcing until it merges into the main branch of the frequency response. This anomaly, often undetected in experimental testing and numerical simulation, can be catastrophic as the response can jump to the stable part of the IRC when excited by an additional input of excitation (initial conditions).

A crucial part of NES design is the choice of nonlinear parameters such that the input excitation level triggers SMR. For a given setup, the excitation limits (i.e. limits of  $P$ ) can be readily estimated and then is scaled with  $\gamma$ , and thereby  $k_{na}$ , to obtain  $\bar{P}$ . This would in-turn provide values for  $Z_b$  and  $Z_a$  for each exciting frequency, from Eqs. (13) and (14), assuming a given  $c_{na}$ . For the region with the SMR response, the choice of the parameter  $c_{na}$  would be to adjust the maxima (Eqs. (15b) and (15c)). Thus, to ensure an optimal SMR response at resonance, both  $c_{na}$  and  $k_{na}$  need to be tuned to overcome the SIM threshold (maxima) for a given  $P$ , while the separation of the SIM limits need to be controlled by  $c_{na}$ . The host system is identified to have properties as in Tab. 1, and for the NES, a value of  $k_{na} = 110 \text{ N rad}^{-3}$  and  $c_{na} = 0.0085 \text{ N rad}^{-1}\text{s}^{-1}$  is chosen after some trial calculations. This will allow the NES to exhibit its typical behavior of SMR, saturation and isola within the force range the benchmark system is able to provide.

$I_1[\text{m}^4]$	$I_2[\text{m}^4]$	$k_1[\text{N rad}^{-1}]$	$k_2 [\text{N rad}^{-1}]$	$c_1 [\text{N rad}^{-1}\text{s}^{-1}]$	$c_2 [\text{N rad}^{-1}\text{s}^{-1}]$
37e-04	125e-04	33.35	17.11	0.0431	0.0085

Table 1: Identified host system parameters

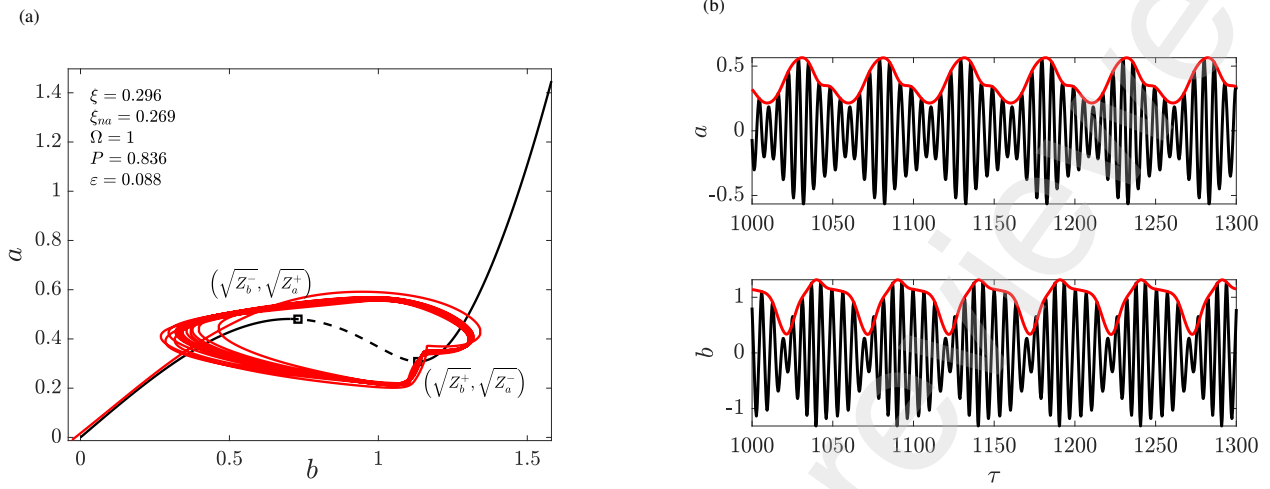


Figure 3: The SIM (black, stable (—) and unstable (---)) with its extrema (□) and an overlay of the actual response envelope (red) obtained from simulations (a), and the corresponding time simulation with the estimated envelope (red) (b)

### 3. Design Methodology

A brief description of the means of inducing nonlinearity in the NES for a practical design is presented, followed by the formulation of an appropriate design optimization problem.

#### 3.1. Conceptual design and piecewise approximation of nonlinearity

The fundamental basis for the NES design is to approximate nonlinear stiffness profiles via a combination of piecewise-linear segments [67]. In this regard, the preliminary design is presented in Fig. 4a. The piecewise-linear torsional stiffness is created by the engagement of flexural rods (axially placed) at different angles on the slotted disc; the slots and rod dimensions are chosen in accordance with the nonlinear profile to be approximated. Furthermore, a number of rods can engage at the same angle, as seen in the figure. Consider a rod made of a material having elastic modulus  $E$ , density  $\rho$ , where each rod  $h$  has a diameter  $d_h$  and length  $L$ . Each of them engages with its corresponding slot at a radial distance of  $R_h$  at intervals  $\theta_h$ , and undergoes a small angular deflection of  $\delta\theta_h$ . Additionally,  $\theta_{max}$  is the maximum displacement allowed in the design. Then the restoring torque  $T_h$  obtained from a single rod is as follows:

$$T_h = \underbrace{\frac{3E \pi d_h^4}{L^3} R_h^2}_{k_{\theta,h}} \underbrace{(\theta - \theta_h)}_{\delta\theta_h} = \frac{3EI_h}{L^3} R_h^2 (\theta - \theta_h) \quad (16)$$

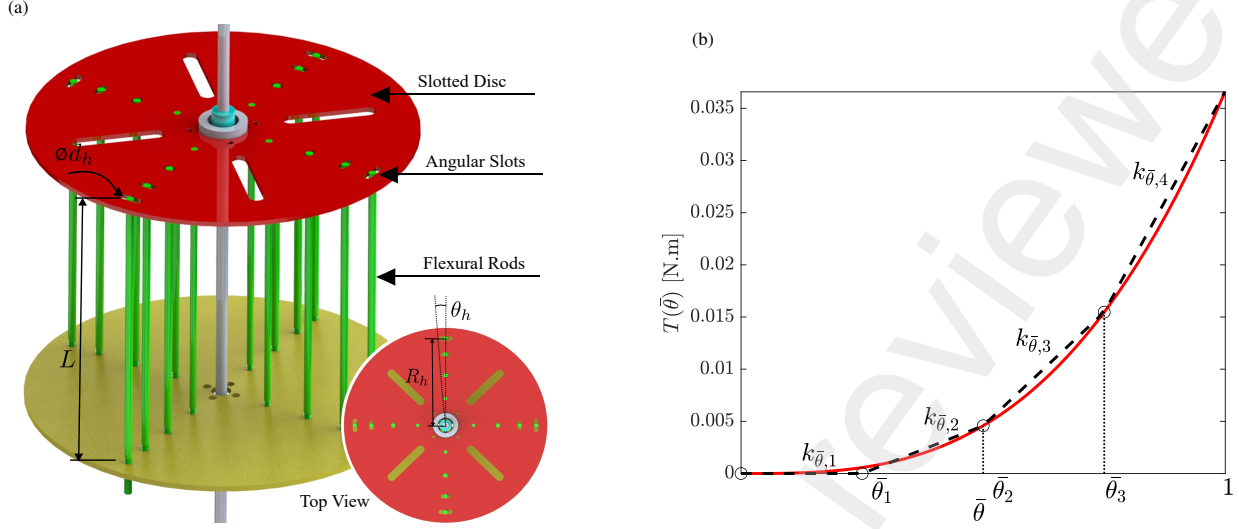


Figure 4: Concept of a piecewise-stiffening NES (a) and comparison (b) of cubic nonlinearity (red, (—)) and its piecewise-linear approximation (black, (- - -)); Note  $\bar{\theta} = \frac{\theta}{\theta_{max}}$  and  $T(-\bar{\theta}) = -T(\bar{\theta})$

Where  $I_h$  is the moment of inertia. The piecewise-linear stiffness function from multiple rod engagements can be written as follows:

$$k_{\theta}(\theta) = \begin{cases} k_{\theta,1} & (|\theta| \leq \theta_1) \\ k_{\theta,1} + k_{\theta,2} & (\theta_1 < |\theta| \leq \theta_2) \\ k_{\theta,1} + k_{\theta,2} + k_{\theta,3} & (\theta_2 < |\theta| \leq \theta_3) \\ k_{\theta,1} + k_{\theta,2} + k_{\theta,3} + k_{\theta,4} & (\theta_3 < |\theta| \leq \theta_{max}) \end{cases} \quad (17)$$

Additionally, the stiffness of each rod  $k_{\theta,h}$  is defined according to the nonlinear stiffness function  $F_{na}(\theta) = k_{na}\theta^3$  as shown in Eq. (18) below. A comparison of the cubic nonlinear stiffness and the approximated piecewise-linear stiffness is shown in Fig. 4b. Note that the stiffness function is symmetric about the origin.

$$k_{\theta,h} = \frac{k_{na}\theta_h^3 - k_{\theta,h-1}\theta_h}{\theta_h - \theta_{h-1}} \quad (18)$$

$$1 \leq h \leq 4; \quad \theta_0 = 0, \quad k_{\theta,0} = 0, \quad \theta_4 = \theta_{max}$$

### 3.2. Material stress and local resonance

A major drawback of a cubic nonlinearity is its need to sustain large displacements (above the threshold limit) to attain the SMR regime. This induces high stresses, making it prone to yielding or vibration-induced fatigue failure. Furthermore, the design should also ensure that local resonances of the rods are avoided, as the stiffness Eq. (16) assumes static deflection of the rods. Each rod in the NES is subjected to two main forces; a tangential force  $F_t$ , which is a point load due to the torque induced by angular deflection of the tip, and a centrifugal force  $F_c$  caused by the angular speed of the rod w.r.t the rotating axis, acting as a uniformly distributed load along its length. The

forces are visualized in Fig. 5. In this setup, the host system's motor is capable of oscillating motion, with maximum

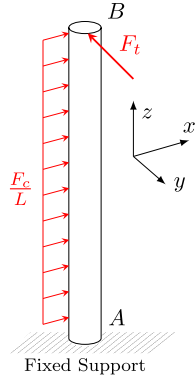


Figure 5: Forces acting on a flexural rod; a tangential point-load  $F_t$  from the torque due to deflection, and a centrifugal uniformly distributed load  $F_c$  from the rotation of the NES.

possible magnitude  $\theta_{2,max}$  observed at  $I_2$  (refer to Fig. 1) and has a maximum rotational frequency  $\omega_{max}$ . For systems that fully rotate, the latter term is equal to the rotational speed. Thus, the centrifugal force  $F_c$  and tangential force  $F_t$  can be defined as in Eq. (19) below.

$$F_c = \rho \underbrace{\frac{\pi d_h^2}{4} L}_{m_h} R_h (\theta_{2,max} \omega_{max})^2 \quad (19)$$

$$F_t = \frac{3E \pi d_h^4}{L^3 64} R_h (\theta_{2,max} - \theta_h)$$

Here,  $F_c$  is calculated for a given rod of mass  $m_h$  at its highest possible magnitude of angular velocity  $\theta_{2,max} \omega_{max}$ , and  $F_t$  is defined as  $\frac{T_h}{R_h}$ . The bending moment and thus, the bending stress would be maximum at A (refer to Fig. 5) and is given by Eq. (20).

$$\sigma_{max,A} = \frac{32 \left( \sqrt{(F_t L)^2 + \left(\frac{F_c L}{2}\right)^2} \right)}{\pi d_h^3} \quad (20)$$

A sufficiently accurate estimation of the first eigenfrequency could be obtained from the Rayleigh Quotient method. This assumes that the rods behave as a static elastic element. For this to hold, it should be avoided that the rods themselves are excited near their natural frequency. The response is defined in Eq. (21) and the assumed spatial eigenfunction  $\psi_n(x)$  is then taken according to mode  $n$  under consideration, as in Eq. (22).

$$y(x, t) = \psi_n(x) \phi_n(t) = \psi_n(x) \sin(\omega_n t + \alpha) \quad (21)$$

Since the first eigenfrequency is being considered we have,

$$\psi_1(u) = \frac{1}{2} (3u^2 - u^3), \quad u = \frac{x}{L}; \quad 0 \leq u \leq 1 \quad (22)$$

Here  $\psi_1(u)$  is approximated as the deflection shape for a static deflection of the rod. The Rayleigh Quotient ( $R$ ) is found taking into account the conservation of energy in the system, i.e. maximum kinetic energy is equal to the

maximum potential energy.

$$R(\psi_1(u)) = \omega_1^2 = \frac{\int_0^1 EI (\ddot{\psi}_1)^2(u) du}{\int_0^1 \rho A \psi_1^2(u) du} = \frac{35 d_h^2 E}{44 \rho L^4} \quad (23)$$

Where  $(\ddot{\cdot}) = \frac{d^2(\cdot)}{du^2}$ , and  $f_1 = \frac{\omega_1}{2\pi}$  is the natural frequency of a flexural rod.

#### 4. Design optimization

A general design optimization procedure is developed with the principle idea of minimizing the bending stress in the rods and avoiding local resonances, while keeping the stiffness profile the same as the desired one. The design variables are the diameters of the rods and their length, and therefore Eqs. (16), (20) and (23) are parametrized with these variables. However, based on the host system's requirements and limitations, certain constraints on the absorber dimensions are also placed. With these under consideration, we can formulate an optimization problem as follows:

$$\begin{aligned} & \text{minimize} && \sigma_{max,A,h}(d_h, L) \\ & \text{subject to} && f_{1,h}(d_h, L) \geq 1.25 f_{max} \\ & && d_{h,min} \leq d_h \leq d_{h,max} \\ & && L_{min} \leq L \leq L_{max} \\ & && R_{h,min} \leq R_h \leq R_{h,max} \end{aligned} \quad (24)$$

Here, the objective function to minimize is the maximum stress of each rod (see Eq. (20)). The constraint functions involve keeping the natural frequency 25% above the maximum rotational frequency, and some dimensional restrictions. A visualization of the design space from the above constraints is shown in Fig. 6b. Here, the objective function is represented as a function of the constraint variables,  $L$  and  $R_h$ ; corresponding to the rods of the  $k_{\theta,h}$  stiffness increment. The black dashed lines show the constraints on  $L$  and  $R_h$ , and the red dashed lines indicate the eigenfrequency constraint. Lines of constant diameter  $d_h$  are also plotted, and can be used to indicate its corresponding constraint function. Before performing a numerical optimization, it is recommended to have an understanding of the effect of the design variables upon the objective function. The relative importance of each constraint function can be assessed by their corresponding reduction of the design space, and necessary modifications can be made to their limits.

Apart from design constraints, some design constants have also been considered as in Tab. 2. Each stiffness increment  $k_{\theta,h}$  can be split equally by having identical rods engage at the same angle  $\theta_h$ . The number of engagements (i.e. rods) per stiffness increment can be increased to further lower local stresses and this can be used to avoid infeasible designs. From the linear stiffness calculations in Eq. (18),  $k_{\theta,1} \approx 0$ , thus negating the need for an initial engagement of a rod. Spring steel is chosen as the material for the rod as it possesses a high yield and endurance limit. The maximum rotation of  $\theta_{2,max}$  is limited by the motor of the setup. Note that the limits on  $d_h$  are from manufacturing concerns, while for  $L$  and  $R_h$ , they are from the dimensional constraints of the machine. The numerical optimization is performed in MATLAB using the *fmincon* function and the default algorithm of *interior-point* has been used. The

Design Constants		Design Constants		Design Constraints	
Parameter	Value	Parameter	Value	Parameter	Limits
$E$ [N/m]	2.06e11	$\rho$ [Kg/m <sup>3</sup> ]	8050	$d_h$ [mm]	$\in [3, 12]$
$\theta_{2,max}$ [rad]	0.1	$\Delta\theta_h$ [rad]	0.025	$L$ [mm]	$\in [50, 250]$
rods per $k_{\theta,h}$	3	$f_{max}$ [Hz]	30	$R_h$ [mm]	$\in [29, 100]$
$k_{\theta,1}$	0				

Table 2: Design constants and constraints of the optimization

Rod Index ( $h$ )	$d_h$ [mm]	$L$ [mm]	$R_h$ [mm]	$\sigma_{max,h}$ [MPa]	$f_{1,h}$ [Hz]
1	-	-	-	-	-
2	3.2	248	29.6	36.64	37.36
3	3.4	''	30.8	27.06	36.39
4	3.8	''	31.5	16.15	44.36

Table 3: Optimized design variables and the resulting objective function values

optimization is computationally inexpensive and takes  $\sim 1$  second to complete. The results of the optimization are presented in Tab. 3. It should be noted that since the manufacturing tolerance is about 0.1 mm, the results have been rounded accordingly. The optimal design obtained has significantly lower rod stress than the material endurance limit ( $\sim 500$  MPa), thus theoretically guaranteeing infinite life for the design. The optimized design thus obtained has been further designed in detail for implementation, as seen in Figs. 6a and 6c.

## 5. Analytical results and Experimental validation

In this section, the harmonic response prediction from CxA (Eqs. (13) and (14)) is compared to experimental results to explore the general agreement between the results obtained and also to validate the choice of the nonlinearity and its parameter value. The parameter values from the NES and from the identification of the primary system is given in Tab. 4. A sine sweep signal from 5.5 Hz to 8 Hz frequency and of amplitude 0.5, 0.6 or 0.75 rad is provided by

$\varepsilon$	$\xi$	$\gamma$	$\omega_1$ [rad/s]	$\xi_{na}$	$P$
0.088	0.296	82.68	42.4	0.269	0.836

Table 4: Parameters of the NES and the identified primary system

the motor to  $I_1$  of the host system (refer to Fig. 6a). The angle measurements are acquired by belt-driven encoders

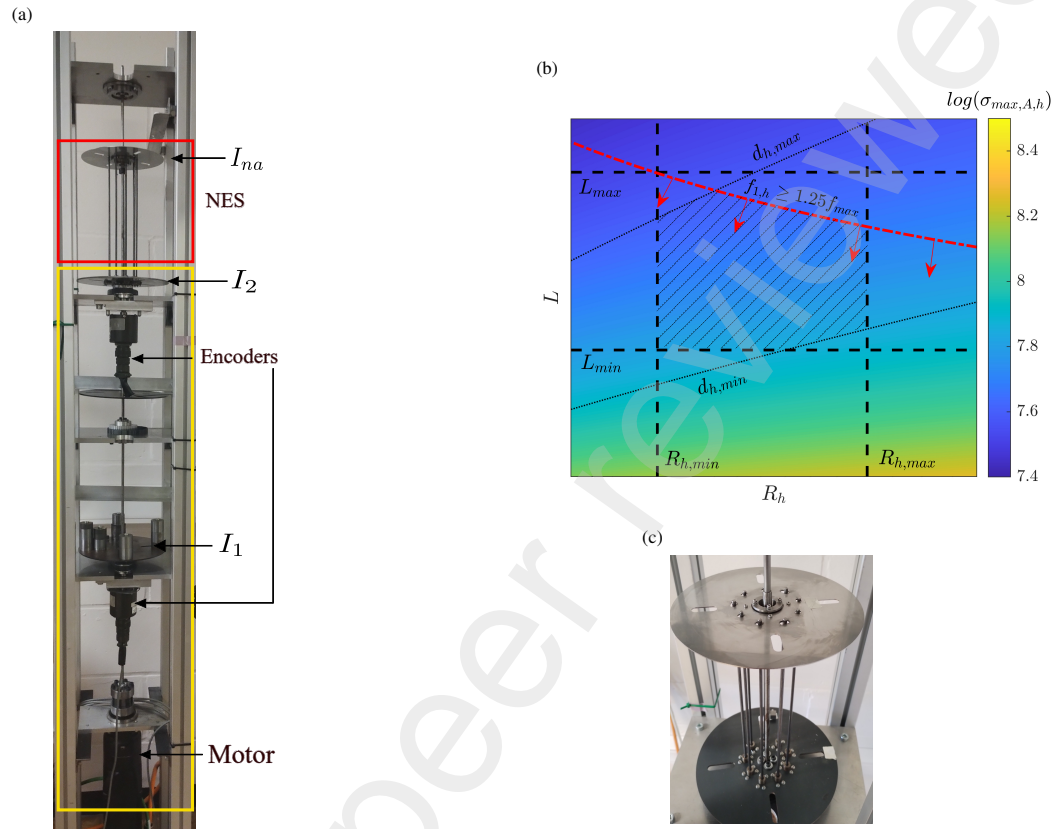


Figure 6: NES assembled onto the 2-DOF benchmark system(a), Visualization of the constrained design space (hatched) with the objective function indicated by the colorbar(b), and assembly of the optimized NES (c)

attached to each of the respective inertias. The measurement data is then filtered, and the envelope of oscillation is then extracted. For visual clarity, the envelope of SIM maxima ( $\sqrt{Z_a^+}$  from Eq. (15c)) is used for regions of quasi-periodic response. The analytical treatment and the experimental measurements are superimposed in Fig. 7. A clear agreement can be seen between the experimental and analytical results, thus validating the CxA method and its assumptions. It can be inferred that for all three excitation cases, there has been a significant reduction and saturation of the resonant response, but with a major caveat; the presence and attachment of an Isolated Resonance Curve (IRC) at higher forcing levels.

For the input excitation of  $\theta_{in} = 0.5$  rad (Fig. 7a), the resonant response (at  $\Omega_1 = 6.75$  Hz) with the NES saturates to around 82% from its undamped value. Complexification-Averaging predicts a region of linear instability at resonance, however, this is due to the response being quasi-periodic in nature, with a modulating envelope as seen in Fig. 3b. The saturation of the measured envelope, indicated by the upper SIM limit is also shown, and it is observed to lie below upper SIM limit predicted by CxA. In a narrow frequency band from 6.1 Hz to 6.2 Hz an IRC is formed, undetected by the experiment.

At  $\theta_{in} = 0.6$  rad (see Fig. 7b), the resonant response is diminished as before ( $\approx 84\%$  reduction), however, the IRC expands to almost merging with the main resonance curve. The response after attachment of the IRC is observed in Fig. 7c for  $\theta_{in} = 0.75$  rad with a large amplitude response predicted by the measurement. Still, this response is lower than the resonant response of the primary system. Also, the saturated resonant response is able to achieve  $\approx 87\%$  vibration suppression. The rise and fall frequency and the response magnitude on the attached curve are also predicted reasonably well by the CxA method. Minor deviations can be attributed to the lack of higher order terms in the ansatz of the proposed CxA solution, as is recommended for high forcing amplitudes. This could also be due to the deviation of the actual, piecewise-linear stiffness, from cubic nonlinear stiffness at high amplitudes. A comparison of the host system's measured response before and after attachment of the NES is shown in Fig. 7d, for a sweep through the resonant frequency. Here, a clear reduction in the response is observed after the attachment, in addition to the saturated quasi-periodic response behavior predicted by the SIM (refer to Fig. 3).

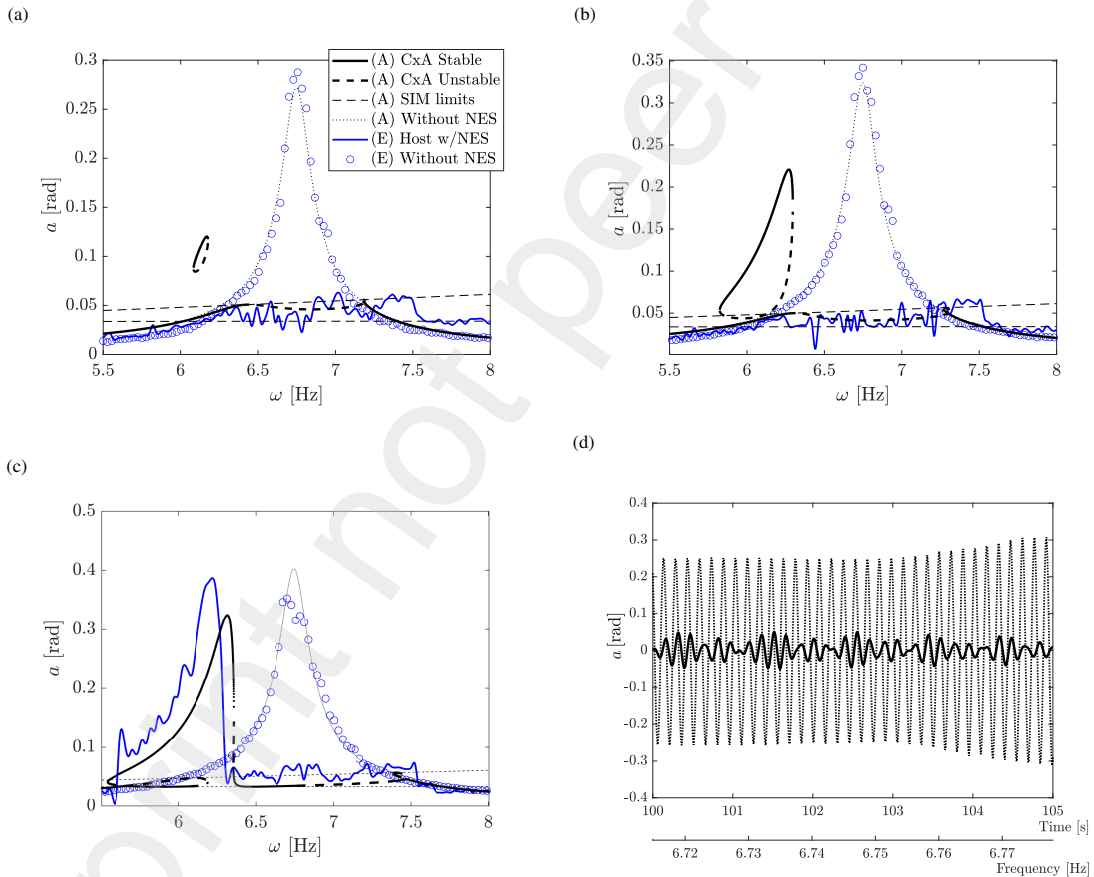


Figure 7: Frequency response of the host system for various input excitations;  $\theta_{in} = 0.5$  rad (a)  $0.6$  rad (b) and  $0.75$  rad (c). The legends (A) indicate the response envelope obtained from CxA with its stable and unstable fixed-points; the SIM limits of the SMR response around 1:1 resonance are also indicated. The experimental validation is indicated by legends (E). The measured time response of the host system (d) with (—) and without NES (.....) for  $\theta_{in} = 0.6$  rad, showing the SMR response around resonance.

## 6. Conclusions

The design and analysis of a piecewise-linear stiffness Nonlinear Energy Sink (NES) for attenuating resonant vibrations in a torsional setup has been successfully explored. The design methodology explained is a complete toolchain that assists the NES implementation by proposing a theoretical framework to obtain an optimal nonlinearity, and then relating it to aspects of structural integrity and practical dimensional restrictions that can be applied to a wide range of systems. An intuitive perspective of the following design optimization is also provided to further understand design parameter influences. The analysis has been implemented with the Complexification-Averaging (CxA) method and validated via experiments, showing a good agreement between them. This supports the use of CxA, even in its first-order, as a suitable method for analyzing systems with strong nonlinearity. Additionally, the CxA method could also detect the presence of an Isolated Resonance Curve (IRC) in the frequency response, undetected by the experimental tests. This added benefit helps to better design by avoiding potential catastrophic responses. At high forcing amplitudes, the IRC attaches to the main resonance curve and this has also been identified by both experiment and CxA response envelopes.

The implemented NES prototype offers a significant attenuation of the resonant response (80% - 87%) for a broad range of input excitation, but its performance is limited at high forcing by the presence and enlargement of an IRC at a sub-resonant frequency band. However, even in this case, the response amplitude is lesser than that of the unattenuated primary system resonance. To avoid IRCs then necessitates a careful design methodology wherein design parameter influences on the inception of the IRC curve are also taken into account. Another scope of further research would be to investigate multi-modal resonance attenuation capability of the NES, and also its potential for absorbing shock loads. Nonetheless, the NES design toolchain can be easily adapted to changing requirements and supports a direct implementation on a torsional host system.

## Appendix A. Stability of slow flow dynamics

The stability of the asymptotic solution of Eq. (11) is computed from the linear stability around equilibrium of  $A$  and  $B$ :

$$2j\sqrt{X} \begin{bmatrix} \dot{\Delta}_A \\ \dot{\Delta}_A^* \\ \dot{\Delta}_B \\ \dot{\Delta}_B^* \end{bmatrix} = \underbrace{\begin{bmatrix} a_{11} & a_{12} & a_{13} & a_{14} \\ a_{21} & a_{22} & a_{23} & a_{24} \\ a_{31} & a_{32} & a_{33} & a_{34} \\ a_{41} & a_{42} & a_{43} & a_{44} \end{bmatrix}}_{\Sigma} \begin{bmatrix} \Delta_A \\ \Delta_A^* \\ \Delta_B \\ \Delta_B^* \end{bmatrix} \quad (\text{A.1})$$

Where  $\Delta_A = A - A_{\text{eq}}$ ,  $\Delta_B = B - B_{\text{eq}}$ . The equilibrium values are found from steady-state Eqs. (11). The matrix elements are described below:

$$\begin{aligned}
 a_{12} &= a_{21} = a_{32} = a_{41} \\
 a_{11} &= -a_{22}^* = -\varepsilon\sigma - j\varepsilon\xi\sqrt{X} \\
 a_{13} &= -a_{24}^* = j\varepsilon\xi_{na}\sqrt{X} + 6\varepsilon BB^*|_{B=B_{\text{eq}}} \\
 a_{14} &= -a_{23}^* = 3\varepsilon B^2|_{B=B_{\text{eq}}} \\
 a_{31} &= -a_{42}^* = \varepsilon\sigma + j\varepsilon\xi\sqrt{X} + X \\
 a_{33} &= -a_{44}^* = X - \frac{1+\varepsilon}{\varepsilon}a_{13} \\
 a_{34} &= -a_{43}^* = -\frac{1+\varepsilon}{\varepsilon}a_{14}
 \end{aligned} \tag{A.2}$$

The stability is then determined from the eigenvalues of  $\frac{\Sigma}{2j\sqrt{X}}$ .

## Appendix B. Stability of SIM

The stability of the solutions on the SIM are computed with the 2nd equation (11). Linearizing this equation around equilibrium  $B_{\text{eq}} = \frac{b}{2}e^{j\beta}$  obtained from the solutions of Eq. (13) gives the following set of equations:

$$\begin{bmatrix} \dot{\Delta}_B \\ \dot{\Delta}_B^* \end{bmatrix} = \underbrace{\begin{bmatrix} a_{11} & a_{12} \\ a_{21} & a_{22} \end{bmatrix}}_{\Sigma} \begin{bmatrix} \Delta_B \\ \Delta_B^* \end{bmatrix} \tag{B.1}$$

where  $\Delta_B = B - B_{\text{eq}}$  and

$$\begin{aligned}
 a_{11} &= a_{22}^* = -\frac{j}{2} - \frac{\xi_{na}}{2} + \frac{j}{2} 6\varepsilon BB^*|_{B=B_{\text{eq}}} \\
 a_{12} &= a_{21}^* = \frac{j}{2} 3\varepsilon B^2|_{B=B_{\text{eq}}}
 \end{aligned} \tag{B.2}$$

Finally, the stability is determined by computing the eigenvalues of  $\Sigma$  matrix in equation (B.1). If any eigenvalue has a positive real part, the solution is unstable.

## References

- [1] C. S. Keeney, S. Shih, Prediction and control of heavy duty powertrain torsional vibration, SAE transactions (1992). doi:10.4271/922481.
- [2] L. S. Dorfman, M. Trubelja, Torsional monitoring of turbine-generators for incipient failure detection, in: Proceedings of the 6th EPRI Steam Turbine/Generator Workshop, Citeseer, 1999, pp. 1–6.
- [3] M. A. Corbo, C. P. Cook, Torsional vibration analysis of synchronous motor-driven turbomachinery, in: Proceedings of the 29th Turbomachinery Symposium, 2000, pp. 161–176. doi:10.21423/R1H37M.
- [4] L. Beneduce, G. Caruso, D. Iannuzzi, F. Maceri, E. Pagano, L. Piegari, Analysis of a structural failure mode arising in cage rotors of induction machines, Electrical Engineering 93 (2011) 179–191. doi:10.1007/s00202-011-0204-8.
- [5] S. Luo, S. Wu, Fatigue failure analysis of rotor compressor blades concerning the effect of rotating stall and surge, Engineering Failure Analysis 68 (2016) 1–9. doi:10.1016/j.engfailanal.2016.05.021.

- [6] H. Frahm, Device for damping vibrations of bodies, 989958, United States (1911).
- [7] J. P. Den Hartog, Mechanical vibrations, Courier Corporation, 1985.
- [8] N. Olgac, B. Holm-Hansen, Tunable Active Vibration Absorber: The Delayed Resonator, *Journal of Dynamic Systems, Measurement, and Control* 117 (4) (1995) 513–519. doi:10.1115/1.2801108.
- [9] S. M. R. Rasid, T. Mizuno, Y. Ishino, M. Takasaki, M. Hara, D. Yamaguchi, Design and control of active vibration isolation system with an active dynamic vibration absorber operating as accelerometer, *Journal of Sound and Vibration* 438 (2019) 175–190. doi:10.1016/j.jsv.2018.09.037.
- [10] X. Wang, B. Yang, Transient vibration control using nonlinear convergence active vibration absorber for impulse excitation, *Mechanical Systems and Signal Processing* 117 (2019) 425–436. doi:10.1016/j.ymssp.2018.07.038.
- [11] K. Kraus, Z. Šika, P. Beneš, J. Krivošej, T. Vyhliđal, Mechatronic robot arm with active vibration absorbers, *Journal of Vibration and Control* 26 (13-14) (2020) 1145–1156. doi:10.1177/1077546320918488.
- [12] J.-H. Koo, M. Ahmadian, M. Setareh, T. Murray, In Search of Suitable Control Methods for Semi-Active Tuned Vibration Absorbers, *Journal of Vibration and Control* 10 (2) (2004) 163–174. doi:10.1177/1077546304032020.
- [13] X. Liu, X. Feng, Y. Shi, Y. Wang, Z. Shuai, Development of a Semi-Active Electromagnetic Vibration Absorber and Its Experimental Study, *Journal of Vibration and Acoustics* 135 (051015) (Jun. 2013). doi:10.1115/1.4023952.
- [14] F. Weber, Semi-active vibration absorber based on real-time controlled MR damper, *Mechanical Systems and Signal Processing* 46 (2) (2014) 272–288. doi:10.1016/j.ymssp.2014.01.017.
- [15] F. Weber, Optimal semi-active vibration absorber for harmonic excitation based on controlled semi-active damper, *Smart Materials and Structures* 23 (9) (2014) 095033. doi:10.1088/0964-1726/23/9/095033.
- [16] P. Gao, C. Xiang, H. Liu, P. Walker, N. Zhang, Design of the frequency tuning scheme for a semi-active vibration absorber, *Mechanism and Machine Theory* 140 (2019) 641–653. doi:10.1016/j.mechmachtheory.2019.06.025.
- [17] A. Schmidt, *Dual-mass flywheel*, 7082855, United States (2006).
- [18] F. T. Wu, C. C. Cheng, Design and analysis of a speed-dependent torsional vibration absorber, *Proceedings of the Institution of Mechanical Engineers, Part D: Journal of Automobile Engineering* 220 (6) (2006) 763–774. doi:10.1243/09544070JAUTO57.
- [19] M. Zink, M. Hausner, The centrifugal pendulum-type absorber-application, *ATZ worldwide* 111 (2009) 42–47. doi:10.1007/BF03225088.
- [20] N. Ichikawa, T. Suzuki, T. Atsumi, *Crank damper pulley structure for the internal combustion engine of a car*, 4710152, United States (1987).
- [21] Y. Starosvetsky, O. Gendelman, Strongly modulated response in forced 2dof oscillatory system with essential mass and potential asymmetry, *Physica D: Nonlinear Phenomena* 237 (13) (2008) 1719–1733. doi:10.1016/j.physd.2008.01.019.
- [22] O. Gendelman, Y. Starosvetsky, M. Feldman, Attractors of harmonically forced linear oscillator with attached nonlinear energy sink i: description of response regimes, *Nonlinear Dynamics* 51 (2008) 31–46. doi:10.1007/s11071-006-9167-0.
- [23] Dekemele, Kevin, Performance measures for nonlinear energy sinks in mitigating single and multi-mode vibrations : theory, simulation and implementation, Ph.D. thesis, Ghent University (2021).
- [24] A. F. Vakakis, O. V. Gendelman, L. A. Bergman, D. M. McFarland, G. Kerschen, Y. S. Lee, *Nonlinear targeted energy transfer in mechanical and structural systems*, Vol. 156, Springer Science & Business Media, 2008. doi:10.1007/978-1-4020-9130-8.
- [25] D. Quinn, R. Rand, J. Bridge, The Dynamics of Resonant Capture, in: A. K. Bajaj, S. W. Shaw (Eds.), *Advances in Nonlinear Dynamics: Methods and Applications*, Springer Netherlands, Dordrecht, 1995, pp. 1–20. doi:10.1007/978-94-011-0367-1\_1.
- [26] G. Kerschen, Y. S. Lee, A. F. Vakakis, D. M. McFarland, L. A. Bergman, Irreversible Passive Energy Transfer in Coupled Oscillators with Essential Nonlinearity, *SIAM Journal on Applied Mathematics* 66 (2) (2005) 648–679. doi:10.1137/040613706.
- [27] D. Hong, T. L. Hill, S. A. Neild, Understanding targeted energy transfer from a symmetry breaking perspective, *Proceedings of the Royal Society A: Mathematical, Physical and Engineering Sciences* 477 (2251) (2021) 20210045. doi:10.1098/rspa.2021.0045.
- [28] A. F. Vakakis, Inducing passive nonlinear energy sinks in vibrating systems, *Journal of Vibration and Acoustics* 123 (3) (2001) 324–332. doi:10.1115/1.1368883.
- [29] F. Nucera, F. L. Iacono, D. M. McFarland, L. Bergman, A. Vakakis, Application of broadband nonlinear targeted energy transfers for seismic

- mitigation of a shear frame: Experimental results, *Journal of sound and vibration* 313 (1-2) (2008) 57–76. doi:10.1016/j.jsv.2010.01.020.
- [30] N. E. Wierschem, J. Luo, M. Al-Shudeifat, S. Hubbard, R. Ott, L. A. Fahnestock, D. D. Quinn, D. M. McFarland, B. Spencer Jr, A. Vakakis, et al., Experimental testing and numerical simulation of a six-story structure incorporating two-degree-of-freedom nonlinear energy sink, *Journal of Structural Engineering* 140 (6) (2014) 04014027. doi:10.1061/(ASCE)ST.1943-541X.00009.
- [31] A. S. Saeed, M. A. AL-Shudeifat, W. J. Cantwell, A. F. Vakakis, Two-dimensional nonlinear energy sink for effective passive seismic mitigation, *Communications in Nonlinear Science and Numerical Simulation* 99 (2021) 105787. doi:10.1016/j.cnsns.2021.105787.
- [32] J. Fu, S. Wan, P. Zhou, J. Shen, M. Loccufer, K. Dekemele, Effect of magnetic-spring bi-stable nonlinear energy sink on vibration and damage reduction of concrete double-column piers: Experimental and numerical analysis, *Engineering Structures* 303 (2024) 117517. doi:10.1016/j.engstruct.2024.117517.
- [33] B. Bergeot, S. Bellizzi, B. Cochelin, Passive suppression of helicopter ground resonance using nonlinear energy sinks attached on the helicopter blades, *Journal of Sound and Vibration* 392 (2017) 41–55. doi:10.1016/j.jsv.2016.12.039.
- [34] K. Yang, Y.-W. Zhang, H. Ding, T.-Z. Yang, Y. Li, L.-Q. Chen, Nonlinear Energy Sink for Whole-Spacecraft Vibration Reduction, *Journal of Vibration and Acoustics* 139 (021011) (Feb. 2017). doi:10.1115/1.4035377.
- [35] I. P. Wall, M. R. Amoozgar, A. A. Popov, Aeroelasticity of an aircraft wing with nonlinear energy sink, *Aerospace Science and Technology* 155 (2024) 109684. doi:10.1016/j.ast.2024.109684.
- [36] A. Nankali, H. Surampalli, Y. S. Lee, T. Kalma'r-Nagy, Suppression of Machine Tool Chatter Using Nonlinear Energy Sink, in: *ASME 2011 International Design Engineering Technical Conferences and Computers and Information in Engineering Conference*, American Society of Mechanical Engineers Digital Collection, 2012, pp. 1215–1223. doi:10.1115/DETC2011-48502.
- [37] B. Peng, X. Yan, J. Du, Suppress the vibration of tool system in milling process, *AIP Advances* 12 (5) (2022) 055018. doi:10.1063/5.0091935.
- [38] A. E. Mamaghani, S. E. Khadem, S. Bab, Vibration control of a pipe conveying fluid under external periodic excitation using a nonlinear energy sink, *Nonlinear Dynamics* 86 (3) (2016) 1761–1795. doi:10.1007/s11071-016-2992-x.
- [39] Z. Lu, Z. Wang, Y. Zhou, X. Lu, Nonlinear dissipative devices in structural vibration control: A review, *Journal of Sound and Vibration* 423 (2018) 18–49. doi:10.1016/j.jsv.2018.02.052.
- [40] H. Ding, L. Q. Chen, Designs, analysis, and applications of nonlinear energy sinks, *Nonlinear Dynamics* 100 (4) (2020) 3061–3107.
- [41] G. Kerschen, J. J. Kowtko, D. M. McFarland, L. A. Bergman, A. F. Vakakis, Theoretical and experimental study of multimodal targeted energy transfer in a system of coupled oscillators, *Nonlinear Dynamics* 47 (2007) 285–309. doi:10.1007/s11071-006-9073-5.
- [42] D. Qiu, S. Seguy, M. Paredes, Tuned nonlinear energy sink with conical spring: design theory and sensitivity analysis, *Journal of Mechanical Design* 140 (1) (2018) 011404. doi:10.1115/1.4038304.
- [43] K. Dekemele, G. Habib, Inverted resonance capture cascade: modal interactions of a nonlinear energy sink with softening stiffness, *Nonlinear Dynamics* 111 (11) (2023) 9839–9861. doi:10.1007/s11071-023-08423-9.
- [44] S. Zhang, J. Zhou, H. Ding, K. Wang, D. Xu, Fractional nonlinear energy sinks, *Applied Mathematics and Mechanics* 44 (5) (2023) 711–726. doi:10.1007/s10483-023-2984-9.
- [45] S. Zhang, J. Zhou, H. Ding, K. Wang, Micro-vibration mitigation of a cantilever beam by one-third power nonlinear energy sinks, *Aerospace Science and Technology* 153 (2024) 109409. doi:10.1016/j.ast.2024.109409.
- [46] H. Venugopal, K. Dekemele, M. Loccufer, Vibration reduction in an unbalanced rotor system using nonlinear energy sinks with varying stiffness, in: *Proceedings of the 11th IFToMM International Conference on Rotordynamics*, Springer International Publishing, Cham, 2024, pp. 358–373. doi:10.1007/978-3-031-40455-9\_30.
- [47] K. Dekemele, G. Habib, M. Loccufer, The periodically extended stiffness nonlinear energy sink, *Mechanical Systems and Signal Processing* 169 (2022) 108706. doi:10.1016/j.ymssp.2021.108706.
- [48] K. Dekemele, G. Habib, M. Loccufer, Vibration mitigation with a nonlinear energy sink having periodically extended stiffness, in: *ISMA2022 Conference on Noise and Vibration Engineering*, 2022, pp. 4044–405.

- [49] G. Habib, F. Romeo, The tuned bistable nonlinear energy sink, *Nonlinear Dynamics* 89 (1) (2017) 179–196. doi:10.1007/s11071-017-3444-y.
- [50] K. Dekemele, Tailored nonlinear stiffness and geometric damping: Applied to a bistable vibration absorber, *International Journal of Non-Linear Mechanics* 157 (2023) 104548. doi:10.1016/j.ijnonlinmec.2023.104548.
- [51] S. Fang, K. Chen, J. Xing, S. Zhou, W.-H. Liao, Tuned bistable nonlinear energy sink for simultaneously improved vibration suppression and energy harvesting, *International Journal of Mechanical Sciences* 212 (2021) 106838. doi:10.1016/j.ijmecsci.2021.106838.
- [52] L. Chen, X. Liao, G. Xia, B. Sun, Y. Zhou, Variable-potential bistable nonlinear energy sink for enhanced vibration suppression and energy harvesting, *International Journal of Mechanical Sciences* 242 (2023) 107997. doi:10.1016/j.ijmecsci.2022.107997.
- [53] X. Liao, L. Chen, H. Lee, A customizable cam-typed bistable nonlinear energy sink, *International Journal of Mechanical Sciences* 271 (2024) 109305. doi:10.1016/j.ijmecsci.2024.109305.
- [54] Y. cheng Zeng, H. Ding, J.-C. Ji, X.-J. Jing, L.-Q. Chen, A tristable nonlinear energy sink to suppress strong excitation vibration, *Mechanical Systems and Signal Processing* 202 (2023) 110694. doi:10.1016/j.ymsp.2023.110694.
- [55] Y.-c. Zeng, H. Ding, A tristable nonlinear energy sink, *International Journal of Mechanical Sciences* 238 (2023) 107839. doi:10.1016/j.ijmecsci.2022.107839.
- [56] H. Chen, Y. Zeng, H. Ding, S. Lai, L. Chen, Dynamics and vibration reduction performance of asymmetric tristable nonlinear energy sink, *Applied Mathematics and Mechanics* 45 (3) (2024) 389–406. doi:10.1007/s10483-024-3095-9.
- [57] C.-H. Lamarque, O. V. Gendelman, A. Ture Savadkoohi, E. Etcheverria, Targeted energy transfer in mechanical systems by means of non-smooth nonlinear energy sink, *Acta Mechanica* 221 (1) (2011) 175–200. doi:10.1007/s00707-011-0492-0.
- [58] O. V. Gendelman, Bifurcations of nonlinear normal modes of linear oscillator with strongly nonlinear damped attachment, *Nonlinear Dynamics* 37 (2004) 115–128. doi:10.1023/B:NODY.0000042911.49430.25.
- [59] Y. Starosvetsky, O. Gendelman, Vibration absorption in systems with a nonlinear energy sink: Nonlinear damping, *Journal of Sound and Vibration* 324 (3) (2009) 916–939. doi:10.1016/j.jsv.2009.02.052.
- [60] M. Krack, J. Gross, *Harmonic balance for nonlinear vibration problems*, Vol. 1, Springer, 2019. doi:10.1007/978-3-030-14023-6.
- [61] L. I. Manevitch, *Complex Representation of Dynamics of Coupled Nonlinear Oscillators*, Springer US, Boston, MA, 1999. doi:10.1007/978-1-4615-4799-0\_24.
- [62] V. V. Smirnov, L. I. Manevitch, Complex envelope variable approximation in nonlinear dynamics, *Russian Journal Of Nonlinear Dynamics* 16 (2020) 491–515. doi:10.48550/arXiv.2004.08354.
- [63] A. Haris, E. Motato, S. Theodossiadis, H. Rahnejat, P. Kelly, A. Vakakis, L. A. Bergman, D. M. McFarland, A study on torsional vibration attenuation in automotive drivetrains using absorbers with smooth and non-smooth nonlinearities, *Applied Mathematical Modelling* 46 (2017) 674–690. doi:10.1016/j.apm.2016.09.030.
- [64] A. Haris, P. Alevras, M. Mohammadpour, S. Theodossiadis, M. O’Mahony, Design and validation of a nonlinear vibration absorber to attenuate torsional oscillations of propulsion systems, *Nonlinear Dynamics* 100 (2020) 33–49. doi:10.1007/s11071-020-05502-z.
- [65] Y. Cao, Z. Li, J. Dou, R. Jia, H. Yao, An inerter nonlinear energy sink for torsional vibration suppression of the rotor system, *Journal of Sound and Vibration* 537 (2022) 117184. doi:10.1016/j.jsv.2022.117184.
- [66] Y. Cao, H. Yao, H. Li, J. Dou, Torsional vibration dynamics of a gear-shafting system attaching a nonlinear energy sink, *Mechanical Systems and Signal Processing* 176 (2022) 109172. doi:10.1016/j.ymsp.2022.109172.
- [67] Y. Cao, H. Yao, J. Dou, S. Han, Optimal design for torsional vibration suppression of non-smooth NES, *Journal of Mechanical Science and Technology* 36 (11) (2022) 5399–5412. doi:10.1007/s12206-022-1006-9.
- [68] Y. Cao, H. Yao, J. Dou, R. Bai, A multi-stable nonlinear energy sink for torsional vibration of the rotor system, *Nonlinear Dynamics* 110 (2) (2022) 1253–1278. doi:10.1007/s11071-022-07681-3.
- [69] J. Dou, H. Yao, Y. Cao, Z. Wang, Permanent magnet based nonlinear energy sink for torsional vibration suppression of rotor systems, *International Journal of Non-Linear Mechanics* 149 (2023) 104321. doi:10.1016/j.ijnonlinmec.2022.104321.
- [70] J. Dou, Z. Li, Y. Cao, H. Yao, R. Bai, Magnet based bi-stable nonlinear energy sink for torsional vibration suppression of rotor system,

Mechanical Systems and Signal Processing 186 (2023) 109859. doi:10.1016/j.ymsp.2022.109859.

- [71] J. Dou, H. Yao, Y. Cao, S. Han, R. Bai, Enhancement of bistable nonlinear energy sink based on particle damper, *Journal of Sound and Vibration* 547 (2023) 117547. doi:10.1016/j.jsv.2022.117547.
- [72] Y. Cao, G. Yan, J. Lu, W. Zhang, Suppression of multi-modal torsional vibration of the long-shafting rotor system with nonlinear piecewise NES, *International Journal of Non-Linear Mechanics* 159 (2024) 104617. doi:10.1016/j.ijnonlinmec.2023.104617.
- [73] O. V. Gendelman, E. Gourdon, C. H. Lamarque, Quasiperiodic energy pumping in coupled oscillators under periodic forcing, *Journal of Sound and Vibration* 294 (4) (2006) 651–662. doi:10.1016/j.jsv.2005.11.031.
- [74] R. J. Kuether, L. Renson, T. Detroux, C. Grappasonni, G. Kerschen, M. S. Allen, Nonlinear normal modes, modal interactions and isolated resonance curves, *Journal of Sound and Vibration* 351 (2015) 299–310. doi:10.1016/j.jsv.2015.04.035.